V European Conference on Computational Fluid Dynamics
ECCOMAS CFD 2010
J. C. F. Pereira and A. Sequeira (Eds)
Lisbon, Portugal,14-17 June 2010

NUMERICAL MODELING OF A MULTI-MECHANISM DAMAGE FOR CEREBRAL ARTERIAL TISSUE

M. de Luca*

*Politecnico di Milano,
Dipartimento di Matematica, Piazza Leonardo da Vinci 32, 20133, Milan
mariarita.deluca@polimi.it

Key words: Cerebral aneurysm, Cerebral arteries, Weakly compressible materials, Finite element, Continuos damage.

Abstract. *We developed a C++ finite element code for a non-linear multi-mechanism model, that is suitable to represent the mechanical behavior of the healthy arterial wall and early stage cerebral aneurysm formation. A cerebral aneurysm is a localized bulge of the arterial wall, resulting from an initial dilatation.*

The core of the multi-mechanism model is to consider the arterial wall made up two mechanisms, related to its two main passive constituents: elastin and collagen. Histological studies show that the early stage aneurysm formation is associated with the disruption of elastin, that is found fragmented in the arterial wall. From experimental observations, the elastin actively contributes to load bearing even at low deformation level, while the collagen network is in a crimped state in its stress free configuration. For larger deformations, the collagen network stretches out and starts to contribute to the mechanical behavior of the arterial wall. The strain energy of the model is additively composed by two terms, one related to the first mechanism and the other related to the second one. The collagen recruitment happens when a threshold deformation is reached. This threshold is checked at each time step in each element of the computational domain allowing a non-uniform collagen activation across the material. The fragmentation of elastin is modeled by multiplying a damage coefficient with the stress tensor term related to the first mechanism. This damage coefficient gradually decreases from one (first mechanism active) to zero (disappearance of first mechanism) as function of deformation.

The code has been validated on a set of test cases for which an analytical solution is available, showing the expected behavior. Numerical simulations for more realistic geometries have shown that the computational multi-mechanism model is able to capture the non-linearity and inelasticity of the arterial wall, and the early stage aneurysm formation.

1 INTRODUCTION

A cerebral intracranial aneurysm is a focal enlargement of a cerebral artery, characterized by a saccular shape of various dimension, up to 30 mm in diameter [1]. The causes beneath the pathogenesis, enlargement and rupture of cerebral aneurysms are object of considerable debate [2]. Most aneurysms remain asymptomatic until rupture that causes a consequent aneurysmal subarachnoid hemorrhage with incidence of sudden death of the 12 % and rates of fatality from 32 % to 67 % after the hemorrhage [3]. The presence of a cerebral aneurysm can remain unknown if it never undergoes rupture. The prevalence of unruptured aneurysms is not known, but it is estimated to be as high as 5 % of the population [4]. It is obvious the need of understanding the natural history of these lesions in order to prevent or treat them. It is still unclear why aneurysms grow and enlarge, but it is well accepted that haemodynamical and mechanical factors play an important role [5].

New image techniques supply geometrical reconstruction of arterial vessels from Computed Tomography scan [6] [7], suitable to be the substrate for numerical simulations. Many computational works focus on the haemodynamics of blood flow inside the aneurysm [8] [9] [10] [11], while few are devoted to numerical simulation of aneurysm formation and growth [12]. The aim of this work is to implement a new damage multi-mechanism constitutive law for cerebral artery to simulate the early stage of cerebral aneurysm formation. The main feature of the model adopted in this paper is to consider the arterial wall made up two material constituents: elastin and collagen. The mechanical behavior of cerebral arterial wall is based on the strain of these two passive constituents, following the model presented by *Robertson and coworkers*[13] [14] [15].

Histological studies show that the early stage aneurysm formation is associated with the disruption of elastin, that is found fragmented in the arterial wall [16]. From experimental observations, the elastin actively contributes to load bearing, even at low deformation level, while the collagen network is in a crimped state in its stress-free configuration. For larger deformations, the collagen network stretches out and starts to contribute to the mechanical behavior of the arterial wall [17].

The strain energy of the model is here additively composed in two terms, one related to the first component and the other related to the second one. Each constituent can be modeled as *Neo-Hookean* or *exponential* material. Both components are considered weakly compressible [18] so that in the strain energy function appears a term penalizing bulk compression. The resulting balance of linear momentum system is strongly non-linear. The discretization of the computational domain is made of tetrahedra and the finite element formulation is based on linear elements. The corresponding non-linear algebraic system has been solved by Newton-Raphson method with exact Jacobian computation.

2 KINEMATICS OF A MULTI-MECHANISM MODEL

In this section we collect the basic notions of kinematics of continuum mechanics needed to introduce the multi-mechanism theory. In this model we consider two mechanisms: the

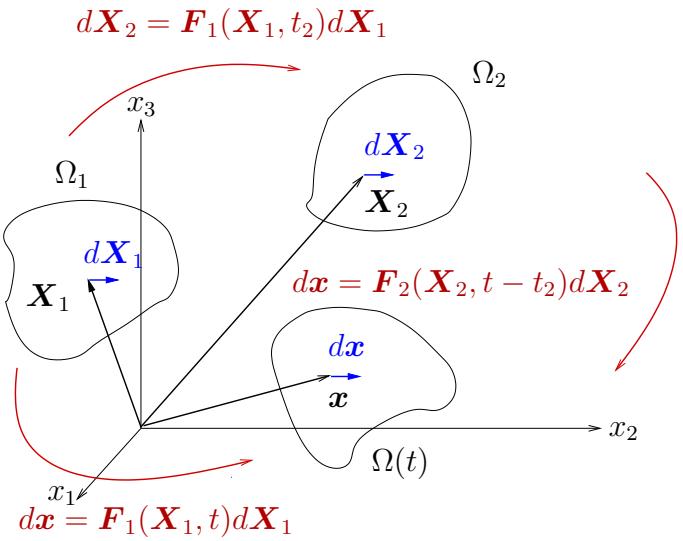

FIGURE 1: The two reference configuration of the model: Ω_1 is related to the elastin mechanism and Ω_2 to the collagen mechanism. $\Omega(t)$ is the current configuration.

elastin component of arterial wall representative of the first mechanism, while the collagen component represents the second mechanism and enters the model when some threshold deformation is reached.

Let us consider a body $\mathscr{B}$, and a bounded domain $\Omega_1 \in \mathbb{R}^3$, which represents the volume occupied by the body in its reference, stress free, configuration. Associated with Ω_1 there is a time reference frame, so that the body is in its reference configuration at time $t = t_1$. At this stage the position of a material point $P_1 \in \Omega_1$ is identified by the vector $\mathbf{X}_1$ as shown in figure 1.

During the motion, the body $\mathscr{B}$ leaves its undeformed state to reach a current configuration $\Omega(t)$, $t > t_1$, where the position vector of a material point is $\mathbf{x} = \boldsymbol{\chi}_1(\mathbf{X}_1, t)$. The vector function $\boldsymbol{\chi}_1(\mathbf{X}_1, t)$ is a smooth, single-valued function, invertible and continuously differentiable with respect to its arguments many times as required. The deformation gradient related to this motion is:

$$\mathbf{F}_1(\mathbf{X}_1, t) = \frac{\partial \mathbf{x}(\mathbf{X}_1, t)}{\partial \mathbf{X}_1} = \frac{\partial \boldsymbol{\chi}_1(\mathbf{X}_1, t)}{\partial \mathbf{X}_1}, \tag{1}$$

where the subscript "1" denotes all the quantities evaluated in the reference configuration Ω_1.

During this first stage of the deformation, only elastin contributes to the mechanical behavior of the body, so that the stress tensor depends only on $\mathbf{F}_1(\mathbf{X}_1, t)$, like a standard elastic material.

The strain energy function W per unit volume, in the reference configuration Ω_1, is

$$W(t) = W_1(\mathbf{F}_1(\mathbf{X}_1, t)). \tag{2}$$

When the body reaches configuration $\Omega_2 = \Omega(t_2)$ the recruitment of collagen fibers occurs. As the body deforms further, corresponding to increased values of deformation, both mechanisms are active and contribute to load bearing. Adopting now Ω_2 as a reference configuration for the second mechanism, a material point position, in such reference configuration, is identified by the position vector:

$$\mathbf{X}_2 = \mathbf{x}(\mathbf{X}_1, t_2) = \boldsymbol{\chi}_1(\mathbf{X}_1, t_2), \tag{3}$$

and, in the current configuration $\Omega(t)$, $t > t_2$, the position of a material particle is represented by the position vector:

$$\mathbf{x} = \boldsymbol{\chi}_2(\mathbf{X}_2, t - t_2), \tag{4}$$

where the vector function $\boldsymbol{\chi}_2(\mathbf{X}_2, t - t_2)$ as well, is a smooth, single-valued function, invertible and continuously differentiable with respect to its arguments many times as required. If we define a new reference time frame t' in Ω_2 such that $t' = t - t_2$, the (4) becomes $\mathbf{x} = \boldsymbol{\chi}_2(\mathbf{X}_2, t')$, and the deformation gradient that describes the motion from the reference configuration Ω_2 is:

$$\mathbf{F}_2(\mathbf{X}_2, t') = \frac{\partial \mathbf{x}(\mathbf{X}_2, t')}{\partial \mathbf{X}_2} = \frac{\partial \boldsymbol{\chi}_2(\mathbf{X}_2, t')}{\partial \mathbf{X}_2}, \tag{5}$$

where now the subscript index "2" denotes all the variables with respect to Ω_2.

An infinitesimal displacement $\mathrm{d}\mathbf{x}$, in the current configuration $\Omega(t)$ can be related to both reference configurations, as follows

$$\mathrm{d}\mathbf{x} = \mathbf{F}_1(\mathbf{X}_1, t)\mathrm{d}\mathbf{X}_1 = \mathbf{F}_2(\mathbf{X}_2, t')\mathrm{d}\mathbf{X}_2. \tag{6}$$

By means of (6) and (3) we can find the relation between the deformation gradients

$$\mathbf{F}_2(\mathbf{X}_2, t') = \mathbf{F}_1(\mathbf{X}_1, t)\, \mathbf{F}_1^{-1}(\mathbf{X}_1, t_2), \tag{7}$$

where the tensor $\mathbf{F}_1^{-1}(\mathbf{X}_1, t_2)$ is known. We can now compute the determinant of each term of equation (7) as

$$\det(\mathbf{F}_2(\mathbf{X}_2, t')) = \det(\mathbf{F}_1(\mathbf{X}_1, t))\ \det(\mathbf{F}_1^{-1}(\mathbf{X}_1, t_2)). \tag{8}$$

If we denote $J_2(t') = \det(\mathbf{F}_2(\mathbf{X}_2, t'))$ and $J_1(t) = \det(\mathbf{F}_1(\mathbf{X}_1, t))$, we have the relation

$$J_2(t') = J_1(t)\left(J_1(t_2)\right)^{-1}, \tag{9}$$

where $\left(J_1(t_2)\right)^{-1}$ is related to the reference configuration Ω_2 and it is a known scalar value constant in time.

The infinitesimal volume transformation among all configurations is

$$\mathrm{d}\Omega(t) = J_1(t)\mathrm{d}\Omega_1 = J_2(t')\mathrm{d}\Omega_2, \tag{10}$$

so that the relation between an infinitesimal volume element in Ω_1 and Ω_2 reads

$$d\Omega_2 = J_1(t)\big(J_2(t')\big)^{-1}\mathrm{d}\Omega_1, \tag{11}$$

and from (9) we finally have

$$d\Omega_2 = J_1(t_2)\mathrm{d}\Omega_1. \tag{12}$$

After collagen recruitment, the strain energy function W associated to the hyperelastic material has contribution from both mechanisms

$$W(t) = W_{1,2}(\mathbf{F}_1(\mathbf{X}_1, t), \mathbf{F}_2(\mathbf{X}_2, t')). \tag{13}$$

When a second critical value of deformation is reached, we hypothesize that elastin starts to degrade, and the first mechanism is weakened.

Before elastin breakage happens, the material behavior is purely elastic, i.e. after unloading it is able to recover the initial configuration Ω_1. After the irreversible damage, the material is no more able to recover the configuration Ω_1 in the unloading stage , but it eventually reaches another reference configuration $\hat{\Omega}$. This configuration depends on the entity of the elastin damage. In particular, when all the elastin is broken, $\hat{\Omega}$ corresponds to Ω_2, only due to relaxed collagen fibers.

W_1 and W_2 have to be invariant with respect to superimposed rigid rotations relative to the correspondent reference configuration Ω_1 and Ω_2. The most general strain energy functions satisfying the invariance requirements are expressed by

$$W_1 = \tilde{W}_1(\mathbf{C}_1), \quad \text{and} \quad W_2 = \tilde{W}_2(\mathbf{C}_2), \tag{14}$$

where $\mathbf{C}_1$ and $\mathbf{C}_2$ are the right Cauchy-Green tensors of the first and second mechanism, respectively

$$\mathbf{C}_1 = \mathbf{F}_1^T\mathbf{F}_1, \quad \text{and} \quad \mathbf{C}_2 = \mathbf{F}_2^T\mathbf{F}_2. \tag{15}$$

With a further hypothesis of isotropy, without loss in generality, the strain energy functions take the form

$$W_1 = \check{W}_1(I_1, II_1, III_1), \quad \text{and} \quad W_2 = \check{W}_2(I_2, II_2, III_2), \tag{16}$$

where (I_1, II_1, III_1) and (I_2, II_2, III_2) are the principal invariants of $\mathbf{C}_1$ and $\mathbf{C}_2$. The isotropy hypothesis is definitely acceptable for elastin mechanism. Collagen fibers are instead arranged with a specific orientation through the arterial wall and we should introduce in W_2 a dependence to account for the anisotropy of fibers [14]. As the focus of this work is the implementation of the multi-mechanism model, at the moment we accept the isotropy hypothesis for collagen too, with future perspective of correcting it.

The last assumption is that the two mechanisms are independent, so that the strain energy function when both elastin and collagen are active is

$$W_{1,2} = W_1 + W_2. \tag{17}$$

Because the two mechanisms represent the behavior of elastin and collagen, respectively, this assumption is largely supported by the fact that both materials are found in distinct layers in the arterial wall [19].

2.1 Strain Energy Function

Let us observe that W_1 and W_2 are strain energy functions per unit volume defined in the reference configuration Ω_1 and Ω_2, respectively. In order to have a complete Lagrangian description in terms of energy of the multi-mechanism model, we need to refer both the energies to only one reference configuration.

By means of (10), the total energy in the current configuration, when both mechanisms are active, is expressed by

$$\mathscr{U}_{tot} = \int_{\Omega(t)} J_1^{-1}(t) W_1 \mathrm{d}\Omega + \int_{\Omega(t)} J_2^{-1}(t') W_2 \mathrm{d}\Omega, \tag{18}$$

such that

$$\mathscr{U}_1 = \int_{\Omega(t)} J_1^{-1}(t) W_1 \mathrm{d}\Omega, \quad \text{and} \quad \mathscr{U}_2 = \int_{\Omega(t)} J_2^{-1}(t') W_2 \mathrm{d}\Omega, \tag{19}$$

and $\mathscr{U}_1$ is the energy associated to the first mechanism and $\mathscr{U}_2$ to the second. If we express the total energy with respect to the reference configuration Ω_1, from equation (18), by means of the relation (12), we have

$$\mathscr{U}_{tot} = \int_{\Omega_1} W_1 \mathrm{d}\Omega_1 + \int_{\Omega_1} J_2^{-1}(t') J_1(t) W_2 \mathrm{d}\Omega_1. \tag{20}$$

The insertion of relation (9) in the previous one gives

$$\mathscr{U}_{tot} = \int_{\Omega_1} W_1 \mathrm{d}\Omega_1 + \int_{\Omega_1} J_1(t_2) W_2 \mathrm{d}\Omega_1, \tag{21}$$

where we recall that $J_1(t_2)$ is known after the collagen recruitment has occurred. If we define W_{tot} as the total strain energy per unite volume in Ω_1, such that

$$\mathscr{U}_{tot} = \int_{\Omega_1} W_{tot} \mathrm{d}\Omega_1, \tag{22}$$

because all the integrals are referred to the volume occupied by the body in the reference configuration Ω_1, when both mechanism are active, we have

$$W_{tot} = W_1 + J_1(t_2) W_2. \tag{23}$$

3 STRESS AND ELASTICITY TENSORS

In this paragraph we introduce the *multiplicative decomposition* of the deformation gradient $\mathbf{F}$ into an *isochoric* (or *distortional*) and a *volumetric* (or *dilational*) part [20] [21] [22], to derive the stress tensors for a weakly compressible material.

The multiplicative decomposition of the deformation gradient $\mathbf{F}$ reads

$$\mathbf{F} = \hat{\mathbf{F}}\overline{\mathbf{F}}, \tag{24}$$

where $\overline{\mathbf{F}} = J^{-\frac{1}{3}}\mathbf{F}$ is the isochoric part, $\hat{\mathbf{F}} = J^{\frac{1}{3}}\mathbf{I}$ is the volumetric part, and $\mathbf{I}$ the identity tensor. The isochoric part of the deformation gradient takes into account the deformation without change in volume, so that $\det\overline{\mathbf{F}} = 1$. The volumetric part contains all the volumetric deformation contributions, and $\det\hat{\mathbf{F}} = J$.

In the same way, we can obtain the multiplicative decomposition of the right Cauchy-Green tensor:

$$\mathbf{C} \;=\; \mathbf{F}^T\mathbf{F} = (\hat{\mathbf{F}}\overline{\mathbf{F}})^T\hat{\mathbf{F}}\overline{\mathbf{F}} = (\overline{\mathbf{F}})^T(\hat{\mathbf{F}})^T\hat{\mathbf{F}}\overline{\mathbf{F}} = J^{\frac{2}{3}}(\overline{\mathbf{F}})^T\overline{\mathbf{F}}, \tag{25}$$

and define the *unimodular* right Cauchy-Green tensors as the isochoric part of $\mathbf{C}$:

$$\overline{\mathbf{C}} = \overline{\mathbf{F}}^T\overline{\mathbf{F}} = J^{-\frac{2}{3}}\mathbf{C}, \quad \text{with} \quad \det\overline{\mathbf{C}} = 1. \tag{26}$$

In particular, together with the invariants of $\mathbf{C}$ we introduce the invariants of $\overline{\mathbf{C}}$ as

$$I_C = \mathrm{tr}\mathbf{C}, \quad II_C = \frac{1}{2}((\mathbf{C})^2 - (\mathrm{tr}\mathbf{C}^2)), \quad III_C = \det\mathbf{C} = J^2, \tag{27}$$

$$I_{\overline{C}} = \mathrm{tr}\overline{\mathbf{C}}, \quad II_{\overline{C}} = \frac{1}{2}((\mathrm{tr}\overline{\mathbf{C}})^2 - \mathrm{tr}(\overline{\mathbf{C}}^2)), \quad III_{\overline{C}} = 1. \tag{28}$$

The use of (24), allows to split the strain energy function for an isotropic frame indifferent material [21] as

$$W(J, I_{\overline{C}}, II_{\overline{C}}) = W_{vol}(J) + W_{iso}(I_{\overline{C}}, II_{\overline{C}}), \tag{29}$$

where:

W_{vol} is a strictly convex function and depends merely on the volume changing part throughout J;

W_{iso} is purely isochoric and depends on the invariants of the unimodular right Cauchy-Green $\overline{\mathbf{C}}$.

In the balance of linear momentum we employ the first Piola-Kirchhoff stress tensor $\mathbf{P}$, hence in the following all the calculation are made in terms of $\mathbf{P}$. If we need to recover

the symmetric Cauchy stress tensor $\boldsymbol{\sigma}$ or the second Piola-Kirchhoff stress tensor $\mathbf{S}$ we may use the relations:

$$\mathbf{S} = \mathbf{F}^{-1}\mathbf{P}, \quad \text{and} \quad \boldsymbol{\sigma} = J^{-1}\mathbf{F}^{T}\mathbf{P}. \tag{30}$$

The introduction of the decomposition (29) allows us to derive the first Piola-Kirchhoff stress tensor for each mechanism as

$$\mathbf{P} = 2\mathbf{F}\frac{dW}{d\mathbf{C}} = 2\mathbf{F}\Big(\frac{dW_{vol}}{d\mathbf{C}} + \frac{dW_{iso}}{d\mathbf{C}}\Big), \tag{31}$$

and the volumetric and isochoric parts of the stress tensor read

$$\mathbf{P}_{vol} = JW'_{vol}\mathbf{F}^{-T}, \tag{32}$$

$$\mathbf{P}_{iso} = 2J^{-2/3}\mathbf{F}\mathbb{P} : \Big(\frac{\partial W_{iso}}{\partial I_{\overline{C}}}\mathbf{I} + \frac{\partial W_{iso}}{\partial II_{\overline{C}}}(I_{\overline{C}}\mathbf{I} - \overline{\mathbf{C}})\Big), \tag{33}$$

where $\mathbb{P} = \mathbb{I} - \frac{1}{3}\mathbf{C}^{-1} \otimes \mathbf{C}$, $\mathbb{I}$ is a fourth order identity tensor, and $\otimes$ denotes the outer tensor product.

Finally, we introduce the fourth order elasticity tensors, obtained by:

$$\mathbb{C}_{vol} = \frac{\mathbf{P}_{vol}}{\partial \mathbf{F}}, \quad \text{and} \quad \mathbb{C}_{iso} = \frac{\mathbf{P}_{iso}}{\partial \mathbf{F}}. \tag{34}$$

3.1 Collagen Recruitment

The collagen recruitment and the elastin breakage are introduced on the basis of an invariant scalar function s that measures the deformation [13]:

$$s(\overline{\mathbf{C}}_1) = \hat{s}(\overline{\mathbf{C}}_1(\mathbf{X}_1, t), \mathbf{x}). \tag{35}$$

If the measure is homogeneous, there is no direct dependence on the position $\mathbf{x}$. During the motion, the collagen recruitment occurs at a threshold value $s = s_a$, and at the corresponding material point, all the collagen fibers are recruited simultaneously. If the deformation is not uniform, the activation criterion can be satisfied at different times in different points of the body; moreover for an inhomogeneous body, s_a will be function of the material position too.

For isotropic materials, we may express s as:

$$s(\overline{\mathbf{C}}_1) = \frac{1}{C_s}W_{1iso}(I_{\overline{C}_1}, II_{\overline{C}_1}), \tag{36}$$

where C_s is a convenient coefficient with dimension of Pa^{-1}.

Finally, by means of the total strain energy function (23), we can express the contribution of both mechanisms in the reference configuration Ω_1 as

$$W_{tot} = \begin{cases} W_1 & \text{for } 0 \le s \le s_a, \\ W_1 + J_1(t_2)W_2 & \text{for } s \ge s_a. \end{cases} \tag{37}$$

The use of equation (29) for a multi-mechanism model leads to split further the energy into W_{1vol} and W_{2vol}, representing the change in volume of the body during the motion, while W_{1iso} and W_{2iso} represent the incompressible contributions of each mechanism. Hence the (37) becomes

$$W_{tot} = \begin{cases} W_{1vol} + W_{1iso} & \text{for } 0 \leq s \leq s_a, \\ W_{1vol} + W_{1iso} + J_1(t_2)(W_{2vol} + W_{2iso}) & \text{for } s \geq s_a. \end{cases} \tag{38}$$

To write the balance of linear momentum in the reference configuration Ω_1 we need to derive the first Piola-Kirchhoff stress tensor of a multi-mechanism. In the following we explicitly indicate the dependence on different time frames when needed for clarity:

$$\mathbf{P}_1(t) = \mathbf{P}(t)_{1vol} + \mathbf{P}(t)_{1\,iso}, \quad \text{and} \quad \mathbf{P}_2(t') = \mathbf{P}(t')_{2\,vol} + \mathbf{P}(t')_{2\,iso}, \tag{39}$$

that, by means of (32) and (33), may be rewritten as:

$$\mathbf{P}(t)_{1\,vol} = J_1(t)\frac{\mathrm{d}W_{1\,vol}}{\mathrm{d}J_1(t)}\mathbf{F}_1^{-T}(t), \tag{40}$$

$$\mathbf{P}(t)_{1\,iso} = 2J_1(t)^{-2/3}\mathbf{F}_1(t)\mathbb{P}_1 : \Big(\frac{\mathrm{d}W_{1\,iso}}{\mathrm{d}\overline{\mathbf{C}}_1}\Big), \tag{41}$$

and

$$\mathbf{P}(t')_{2\,vol} = J_2(t')\frac{\mathrm{d}W_{2vol}}{\mathrm{d}J_2(t')}\mathbf{F}_2^{-T}(t'), \tag{42}$$

$$\mathbf{P}(t')_{2\,iso} = 2J_2(t')^{-2/3}\mathbf{F}_2(t')\mathbb{P}_2 : \Big(\frac{\mathrm{d}W_{2\,iso}}{\mathrm{d}\overline{\mathbf{C}}_2}\Big). \tag{43}$$

To simplify the notation, let us define

$$\mathbf{F}_1(\mathbf{X}_1, t_2) = \mathbf{F}^* \quad \text{and} \quad J_1(t_2) = J^*. \tag{44}$$

hence from (7) and (9), we have

$$\mathbf{F}_2(t') = \mathbf{F}_1(t)(\mathbf{F}^*)^{-1} \quad \text{and} \quad J_2(t') = J_1(t)\,(J^*)^{-1}. \tag{45}$$

The replacement of (45) in (42) and (43) allows us to pull back the first Piola-Kirchhoff of the second mechanism $\mathbf{P}_2$ to the reference configuration Ω_1.

When $\mathbf{P}(t)_{2\,vol}$ and $\mathbf{P}(t)_{2\,iso}$ are expressed with respect to the first reference configuration Ω_1, we may neglect in notation their dependence over time, and the total first Piola-Kirchhoff stress tensor for a multi-mechanism model reads

$$\mathbf{P} = \begin{cases} \mathbf{P}_{1\,vol} + \mathbf{P}_{1\,iso} & \text{for } 0 \leq s < s_a, \\ \mathbf{P}_{1\,vol} + \mathbf{P}_{1\,iso} + J^*(\mathbf{P}_{2\,vol} + \mathbf{P}_{2\,iso}) & \text{for } s > s_a. \end{cases} \tag{46}$$

The stress tensors $\mathbf{P}_1$ and $\mathbf{P}_2$ are strongly non-linear, hence to linearize and solve the balance of linear momentum, we need to compute the fourth order elasticity tensors. By means of (34) we find

$$\mathbb{C}_1 = \frac{\partial \mathbf{P}_1}{\partial \mathbf{F}_1}, \quad \text{and} \quad \mathbb{C}_2 = \frac{\partial \mathbf{P}_2}{\partial \mathbf{F}_1}, \tag{47}$$

where both $\mathbb{C}_1$ and $\mathbb{C}_2$ are obtained deriving $\mathbf{P}_1$ and $\mathbf{P}_2$ with respect to $\mathbf{F}_1$, because both stress tensors refer to the first reference configuration Ω_1.

We observe that in Finite Element Method procedure, the needed quantity is not $\mathbb{C}_1$ or $\mathbb{C}_2$, but their saturation with an increment $\delta\mathbf{F}_1$ of $\mathbf{F}_1$; i.e. the linearization of the stress tensors in the direction of an increment $\delta\mathbf{F}_1$:

$$\mathbb{C}_1 : \delta\mathbf{F}_1 = \frac{\partial \mathbf{P}_1}{\partial \mathbf{F}_1} : \delta\mathbf{F}_1, \quad \text{and} \quad \mathbb{C}_2 : \delta\mathbf{F}_1 = \frac{\partial \mathbf{P}_2}{\partial \mathbf{F}_1} : \delta\mathbf{F}_1. \tag{48}$$

3.2 Elastin Degradation

The first mechanism is associated with the elastin component of arterial wall. As pointed out in section 1, early stage aneurysm formation is hypothesized to be related to a mechanical damage of elastin. Hence, we introduce, in the multi-mechanism model a continuous isotropic damage model for the first mechanism, following the model of *Robertson and coworkers*[15].

We define an internal damage variable $D \in [0, 1]$ and following the approach described in [23] we postulate that the decoupled representation of the first mechanism strain energy function (see equation (29)) still holds for the *free energy*:

$$W_1^D(J, I_{\overline{C}_1}, II_{\overline{C}_1}, D) = W_{1vol}(J) + (1 - D)W_{1iso}(I_{\overline{C}_1}, II_{\overline{C}_1}), \tag{49}$$

where $W_{1vol}(J)$ is the same function defined in section 3 which describes the volumetric elastic response, and $W_{1iso}(I_{\overline{C}_1}, II_{\overline{C}_1})$ is the isochoric effective strain energy of the undamaged material, which describes the isochoric elastic response. We observe that deformations due to temperature changes are neglected. As suggested in [24], the damage phenomenon affects only isochoric deformations. We call $\mathbf{P}_1^D$ the first Piola-Kirchhoff stress tensor of the damage model.

From relation (49), the volumetric part of $\mathbf{P}_1^D$ is

$$\mathbf{P}_{1vol}^D = \mathbf{P}_{1vol}, \tag{50}$$

and from the Clausius-Plank inequality, it follows that [23]:

$$\mathbf{P}_{1iso}^D = (1 - D)\mathbf{P}_{1iso}, \tag{51}$$

$$-\frac{\partial W_1^D}{\partial D}\dot{D} = W_{1iso}\dot{D} \geq 0. \tag{52}$$

Inequality (52) specify that damage is a dissipative and irreversible phenomenon. Moreover W_{1iso} is the thermodynamic conjugate variable of $\dot{D}$, and the evolution of D may be described in terms of W_{1iso}.

Let us consider again the scalar function of deformation $s(\overline{\mathbf{C}}_1(t))$ defined in (36), and consider a threshold s_b below which no damage occurs. We suppose that $s_b > s_a$, where s_a is defined in section 3.1 and represents the scalar measure of deformation at which collagen is recruited. While the body deforms, as long as $s(\overline{\mathbf{C}}_1(t)) < s_b$, elastin damage never occurs and after the unloading stage the body recovers its initial stress-free configuration Ω_1. Once the deformation threshold $s = s_b$ is reached, an irreversible damage to elastin component prevents the body, in the unloading stage, to recover the initial configuration Ω_1 and it will reach another stress-free configuration.

To take into account the gradual irreversible damage of elastin material, we define

$$s^{\max}(\overline{\mathbf{C}}_1(t)) = \max_{0\leq\tau\leq t} s(\overline{\mathbf{C}}_1(\tau)), \tag{53}$$

as the maximum of our measure $s(\overline{\mathbf{C}}_1(t))$ during the history of deformation. At each time step, i.e. at each value of deformation, the quantity

$$\phi(\overline{\mathbf{C}}_1(t)) = s^{\max}(\overline{\mathbf{C}}_1(t)) - s(\overline{\mathbf{C}}_1(t)) = 0 \tag{54}$$

represents a surface in strain space. The normal to this surface is $\mathbf{N}_{iso} = \frac{\partial\phi}{\partial\overline{\mathbf{C}}_1}$; when $\mathbf{N}_{iso} : \delta\overline{\mathbf{C}}_\mathbf{1} > 0$ the strain is increasing (loading stage), otherwise when $\mathbf{N}_{iso} : \delta\overline{\mathbf{C}}_1 < 0$ the strain is decreasing (unloading stage).

The analytic expression of damage variable D in terms of $s^{\max}$ is:

$$D(s^{\max}) = \frac{1}{2}\tanh\frac{s_f - s^{\max}(\overline{\mathbf{C}}_1(t))}{s_f - s_e} + \frac{1}{2}, \tag{55}$$

where s_f and s_e are two scalar parameters, and D depends on $\overline{\mathbf{C}}_1(t)$ through $s^{\max}(\overline{\mathbf{C}}_1(t))$. We observe that when $^{\max} = s_f$, $D(s_f) = 0.5$, i.e. the elastin at the correspondent point is half-degraded, and s_e contains the information about the speed of the damage process.

At each time t, the evolution of the damage is regulated by

$$\dot{D} = \begin{cases} \dfrac{\partial D}{\partial s^{\max}}\dot{s^{\max}} & \text{if } \phi = 0 \text{ and } \mathbf{N}_{iso} : \delta\overline{\mathbf{C}}_1 > 0, \\ \\ 0 \quad \text{otherwise.} \end{cases} \tag{56}$$

Finally, we may represent the first Piola-Kirchhoff stress tensor $\mathbf{P}$ of the full multi-mechanism model with damage as:

$$\mathbf{P} = \begin{cases} \mathbf{P}_{1\,vol} + \mathbf{P}_{1\,iso} & \text{for } 0 \leq s < s_a, \\ \mathbf{P}_{1\,vol} + \mathbf{P}_{1\,iso} + J^*(\mathbf{P}_{2\,vol} + \mathbf{P}_{2\,iso}) & \text{for } s_a < s < s_b, \\ \mathbf{P}_{1\,vol} + (1-D)\mathbf{P}_{1\,iso} + J^*(\mathbf{P}_{2\,vol} + \mathbf{P}_{2\,iso}) & \text{for } s \geq s_b. \end{cases} \tag{57}$$

As $\mathbf{P}_{1\,vol}$ and $\mathbf{P}_{2\,vol}$ have the role of penalizing the material compression, they do not have a specific constitutive meaning for the multi-mechanism model. Hence, to simplify the equation, we consider only one volumetric contribution:

$$\mathbf{P}_{vol} = \mathbf{P}_{1\,vol}, \tag{58}$$

and rewrite equation (57) as

$$\mathbf{P} = \mathbf{P}_{vol} + \begin{cases} \mathbf{P}_{1\,iso} & \text{for } 0 \leq s < s_a, \\ \mathbf{P}_{1\,iso} + J^* \mathbf{P}_{2\,iso} & \text{for } s_a < s < s_b, \\ (1-D)\mathbf{P}_{1\,iso} + J^*(\mathbf{P}_{2\,iso}) & \text{for } s \geq s_b. \end{cases} \tag{59}$$

From (47), the fourth order isochoric elasticity tensor is:

$$\mathbb{C}^D_{1\,iso} = \frac{\partial\left((1-D)\mathbf{P}_{1\,iso}\right)}{\partial \mathbf{F}_1}, \tag{60}$$

and the linearization of the first Piola-Kirchhoff stress tensor for a first mechanism with damage is

$$\mathbb{C}^D_{1\,iso} : \delta\mathbf{F}_1 = -D\,\mathbb{C}_{1\,iso} : \delta\mathbf{F}_1 + \frac{\partial D}{\partial s}(\mathbf{P}_{1\,iso} \otimes \mathbf{P}_{1\,iso}) : \delta\mathbf{F}_1, \tag{61}$$

where $\mathbb{C}_{1\,iso} = \dfrac{\partial \mathbf{P}_{1\,iso}}{\partial \mathbf{F}_1}$.

3.3 Material Parameters

The analytic expressions of the strain energy functions employed are:

$$W_{vol} = \frac{K}{4}((J_1-1)^2 + (\ln J_1)^2), \tag{62}$$

$$W^{\mathrm{NH}}_{1\,iso} = \frac{\mu_1}{2}(I_{\overline{C}_1} - 3), \tag{63}$$

$$W^{\mathrm{Exp}}_{j\,iso} = \frac{\alpha_j}{2\gamma_j}(\mathrm{e}^{\gamma_j (I_{\overline{C}_j} - 3)} - 1), \quad \text{with} \quad j = 1, 2. \tag{64}$$

The strain energy functions adopted herein is the sum of the volumetric contribution (62) [21] plus an isochoric contribution. As suggested in the literature[13], for the first mechanism the choices are both (63) and (64), while only the exponentian strain energy function (64) is suitable for the second mechanism.

The material parameters used for the double-mechanism are taken from the literature[14] and are listed in table 1.

	Neo-Hook	Exponential
1st Mech.	$\mu_1 = 27.68\,10^5$ Pa	$\alpha_1 = 7.12$ KPa, $\gamma_1 = 0.86$
2nd Mech.	-	$\alpha_2 = 31.28$ KPa, $\gamma_2 = 1.87$

TABLE 1: Table of material parameters used in strain energy functions (62, 63, 64).

The volumetric coefficient K (bulk modulus) of the strain energy function (see expression (62)) cannot be measured by experiments. It multiplies the volumetric part of the

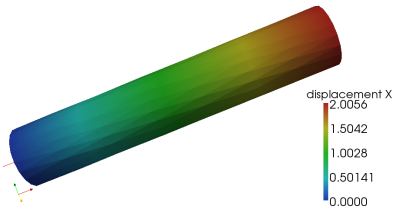

(a) Example of the tension test carried on a cylinder with the isochoric Neo-Hookean constitutive law for a single-mechanism. The color scale represents the displacement in the axis direction (x). Scrolling is allowed on the lower base of the cylinder.

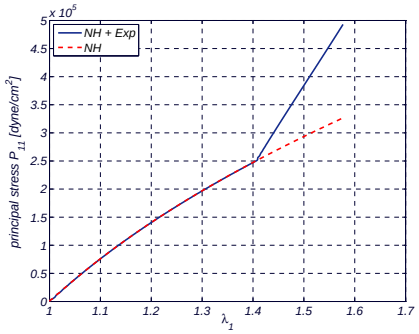

(b) Comparison between the stress-strain graph for a tension test with a single and a double mechanism law. The blue line is the behavior of a double Neo-Hook and Exponential model, and the red dashed line in a single Neo-Hookean model. The two curves are overlapped until the deformation threshold activates the exponential collagen mechanism.

FIGURE 2: Tension test in case of uniform deformations.

strain energy function, giving rise to a penalization term, that allows the material only slight compression. In *Le Tallec* [25], we find the suggestion that it should be in the range:

$$C_s\, 10^2 \leq K \leq C_s\, 10^6, \tag{65}$$

where C_s is the characteristic shear modulus of the material. For smaller values of K there is loss of accuracy in computing the solution and for larger values the condition number of the associated discrete linear system becomes too large.

In this work we use for the bulk modulus the value $K = 10^7$ Pa, that is included in range (65) when $C_s = \mu_1$ or $C_s = \alpha_1$.

4 NUMERICAL RESULTS AND DISCUSSION

Some simple numerical tests have been used to explain the behavior of the collagen recruitment mechanism within the double mechanism model in the case of uniform deformations and non-uniform deformations. The tests are performed as a series of quasi-static deformations.

We consider a cylinder, the upper surface is posed in traction, linearly varying with time, the lateral surface is stress free, and the homogeneous Dirichlet boundary conditions are imposed at the component of displacement along the cylinder axis x on the lower surface. The initial length of the cylinder is 1 cm and its radius 0.5 cm. A picture of the deformed cylinder is shown in figure 2(a).

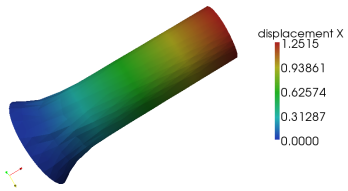

(a) Example of a tension test carried on the cylinder with the isochoric Neo-Hook constitutive law for a single-mechanism. The color scale represents the displacement in the axis direction (x). The lower base of the cylinder is now locked.

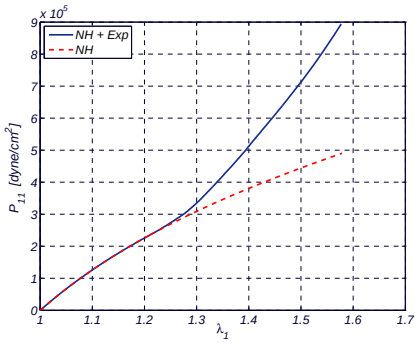

(b) Comparison between the stress-strain graph for a tension test with a single and a double mechanism law. The blue line is the behavior of a double Neo-Hook and Exponential model, and the red dashed line in a single Neo-Hookean model. The two curves smoothly separates because the collagen recruitment is gradual throughout the cylinder.

FIGURE 3: Tension test in case of non-uniform deformations.

In this test, the deformation is uniform, i.e. it is the same in each point. Therefore, the deformation threshold $s_a = 0.5$ is reached contemporaneously by all elements of the computational domain. In figure 2(b) is shown a comparison of the stress-strain curve obtained with a double-mechanism and a single-mechanism model. The deformation λ_1 is computed as the current length over the initial length of the cylinder and the stress P_{11} is the principal first Piola-Kirchhoff stress component in the axial direction x. The double-mechanism, composed by a Neo-Hookean material for the first mechanism and an Exponential material for the second, is compared with a single Neo-Hookean material. It can be observed, in figure 2(b), that the two curves overlap until the threshold value is reached (which corresponds to $s = s_a$). Above such value, they are different. As a matter of fact at $s = s_a$ the second mechanism becomes active in all the points of the cylinder.

To test the behavior of the double-mechanism model in case of non-uniform deformation, we modify the previous tension test imposing a Dirichlet homogeneous boundary condition on all the components of displacement at the lower base of the cylinder (see figure 3(a)).

In this case, the deformation is not the same in all the points of the cylinder. As the deformation is not uniform, at each time only some elements are activated. In figure 3(b) we plot P_{11}, the first Piola-Kirchhoff stress component in the axial direction x, versus the deformation λ_1, computed as in the previous test. The blue curve represents

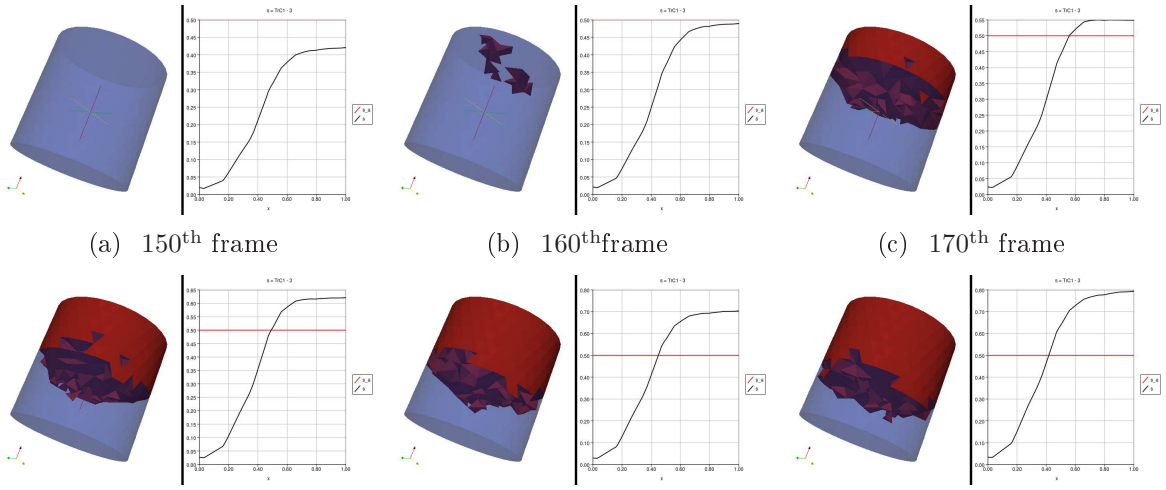

(a) 150^{th} frame (b) 160^{th}frame (c) 170^{th} frame

(d) 180^{th}frame (e) 190^{th} frame (f) 200^{th}frame

FIGURE 4: The picture shows the highlighting of activated elements at different time, i.e. at different values of traction, and the correspondent graph of scalar measure of deformation $s = \frac{1}{\mu_1} W_{1\,iso}^{NH}$, along the axis x, with respect to the activation threshold $s_a = 0.5$. The activated elements are plotted on the initial geometry.

a double-mechanism made of a Neo-Hookean and and Exponential material, and the red dashed curve is a single Neo-Hookean mechanism. In this case, we observe that before the collagen recruitment, the two curves are overlapped, but the split-up is very smooth, due to the fact that the second mechanism becomes active smoothly within the elements of the computational domain.

We notice that for large enough traction, the deformation overcomes the threshold, starting from the elements of the upper surface and then in rest of the cylinder. Correspondingly, in figures 4, the activation of the elements belonging to the upper surface of the cylinder occurs earlier than the activation of the elements below them. In figures 4, activated elements at different time frame, i.e. at different values of traction, are highlighted on the initial geometry. Each picture is joined by the corresponding graph of the scalar measure of deformation $s = \frac{1}{\mu_1} W_{1\,iso}^{NH}$, along the cylinder axis x, with respect of the activation threshold $s_a = 0.5$.

To show the behavior of the full multi-mechanism damage model, we consider an inflation test carried on a straight tube, representing a portion of an artery, where the inner radius is decreasing along the axis. This geometrical feature may represent an initial non healthy situation of the artery. The inflation test has been performed as a series of quasi static inflation, increasing the internal pressure linearly with time. The length of the tube is 3 cm, the minimum and maximum inner radius are 0.3 and 0.1 cm, and the outer radius is 0.5 cm. The parameters used are $s_a = 0.5$, for collagen activation, $s_e = 1.15$,

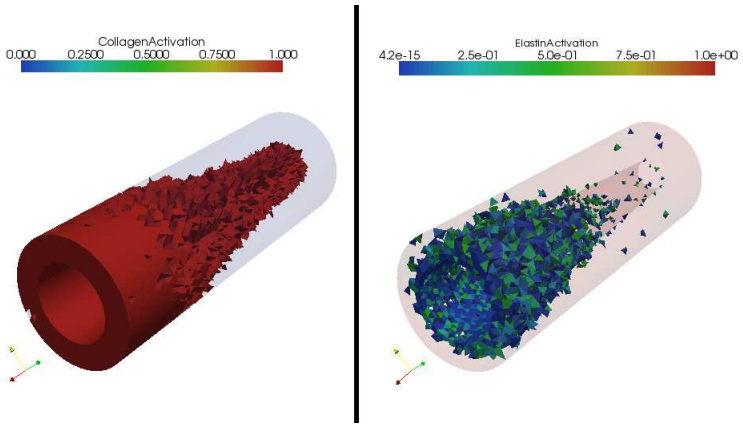

FIGURE 5: Picture of activated collagen elements (left) and damaged elastin elements (right) for an inflation test of a straight tube with narrowing radius. The final inflation pressure is 31 KPa.

and $s_f = 1.1$ for the elastin damage model.

The inflation of the cylinder induces a non-uniform deformation within the tube. In particular, the deformation is maximum at the inner of the cylinder and radially decreases. We observe that where the arterial wall is thicker the deformation is smaller, and the subsequent activation of collagen involves only few elements close to the lumen, while where the wall is thinner, the deformation is wider and all the collage elements are activated, see the red elements in left figure 5. Right figure 5 shows the elements in which the elastin is damaged. As for the collagen, we observe that where the arterial wall is thinner, the deformation is bigger and the damage of elastin elements happens before than in the rest of the tube.

In particular, where the elastin is damaged, the wall becomes even weaker and the deformations larger. In figure 6 we show the comparison between the reference geometry and the deformed geometry. In particular the deformation of the portion of the tube where the elastin is damaged may be very similar to the initial stage of an aneurysm formation.

5 CONCLUSION AND DISCUSSION

In this paper we present the implementation and numerical results obtained with a multi-mechanism model suitable to simulate the non-linear and complex behavior of cerebral arteries. The theoretical model was first presented by *Robertson and coworkers* [14] [15] [13].

The big challenge of this model is the need of two reference configurations for elastin and collagen. Our contribution to the multi-mechanism model is the derivation of the Lagrangian formulation of the whole constitutive model in the first (elastin) reference configuration. Hence, it has been necessary to map the stress tensor of the collagen

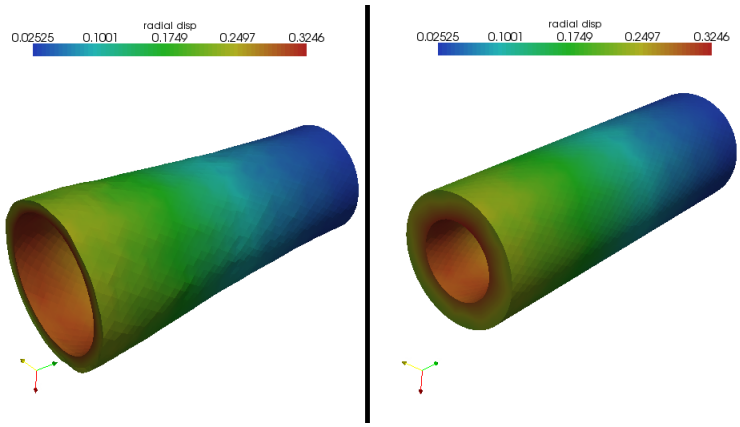

FIGURE 6: Comparison between the reference geometry and the deformed geometry for an inflation test of a straight tube with narrowing radius.

mechanism to the elastin reference configuration. The resulting non standard formulation required a particular attention in the code implementation. The final non-linear system has been solved by means of Newton-Raphson method with exact jacobian computation [28]. The multi-mechanism model presented in this paper has been implemented in non-commercial Finite Element library LifeV [29].

The numerical results obtained with our solver show that the multi mechanism model is able to capture the non-linear characteristics of arterial wall. At low level of deformation the elastin (first mechanism) supplies weak resistance to the tension test, while when the collagen enters the model, it renders the whole material stiffer. We showed that the way the collagen is recruited depends on a very general way by the deformation field.

Finally a more realistic inflation test has been shown. In this numerical simulation, we observe that the collagen recruitment and elastin deactivation start from the lumen of the arteries, where the deformation is wider. In particular, the narrowing of the internal radius of the cylinder, may be interpreted as an initial unhealthy situation, that leads to an non-uniform damage of the elastin mechanism and lead to an enlargement of the arterial segment. From a qualitative point of view the enlargement represents the initial stage of aneurysm formation, due to mechanical damage of elastin components of arterial wall.

Acknowledgements: This work has been carried out in collaboration with Davide Ambrosi, Modeling and Scientific Computing (MOX), Dipartimento di Matematica, Politecnico di Milano; Anne M. Robertson, Department of Mechanical Engineering and Material Science (MEMS), University of Pittsburgh and Alessandro Veneziani, Department of Mathematics and Computer Science, Emory University.

This work has been supported by the ERC Advanced Grant N.227058 MATHCARD,

the project Director Prof. A. Quarteroni.

REFERENCES

[1] K. Matsumoto, Investigation of the surgically treated and untreated unruptured cerebral aneurysms of the anterior circulation. *Surgical Neurology* **60**(6), 516–522 (2003).

[2] J. D. Humphrey and C. A. Taylor, Intracranial and abdominal aortic aneurysms: Similarities, differences, and need for a new class of computational models. *Annu. Rev. Biomed. Eng.* **10**, 221–246 (2008).

[3] J. Huang and J. Van Gelder, The probability of sudden death from rupture of incranial aneurysms: A meta-analysis. *Neurosurgery* **51**(5), 1101–1107 (2002).

[4] H. R. Winn, J. A. Jane, J. Taylor, D. Kaiser, and G. W. Britz, Prevalence of asymptomatic incidental aneurysms: review of 4568 arteriograms. *J. Neurosurgery* **96**(1), 43–49 (2002).

[5] J. D. Humphrey and P. B. Canham, Structure, Mechanical properties, and mechanics of intracranial saccular aneurysms. *Journal of Elasticity* **61** 49–81 (2000).

[6] M. Hernandez, A. F. Frangi, and G. Sapiro, Quantification of brain aneurysm dimensions from CTA for surgical planning of coiling interventions. *Springer US* (2005).

[7] L. Antiga, M. Piccinelli, L. Botti, B. Ene-Iordache, A. Remuzzi, and D. A. Steinman, An image-based modeling framework for patient-specific computational haemodynamics. *Medical and Biological Engineering and Computing* **46**(11) 1097–1112 (2008).

[8] A. Chien, M. A. Castro, S. Tateshima, J. Sayrec, J. Cebral, and F. Viñuela, Quantitative hemodynamic analysis of brain aneurysms at different locations. *American Journal of Neuroradiology* **30** 1507–1512 (2009).

[9] J. R. Cebral, M. A. Castro, J. E. Burgess, R. S. Pergolizzi, M. J. Sheridan, and C. M. Putman, Characterization of cerebral aneurysms for assessing risk of rupture by using patient-specific computational haemodynamics models. *American Journal of Neuroradiology* **26**(10) 2550–2559 (2005).

[10] D. A. Steinman, J. S. Milnera, C. J. Norleya, S. P. Lowniea, and D. W. Holdswortha, Image-based computational simulation of flow dynamics in a giant intracranial aneurysm. *American Journal of neuroradiology* **24** 559–566 (2003).

[11] T. Passerini, Computational haemodynamics of the cerebral circulation: multiscale modeling from the circle of Willis to cerebral aneurysms. *PhD Thesys, Politecnico di Milano* (2009).

[12] P. Watton and Y. Ventikos, Modeling evolution of saccular cerebral aneurysms. *J. Strain Analysis* **44**(5) 375–389 (2009).

[13] R. Wulandana, A. M. Robertson, An Inelastic multi-mechanism constitutive equation for cerebral arterial tissue. *Biomech Model Mechanobiol* **4** 235–248 (2005).

[14] D. Li and A. M. Robertson, A structural multi-mechanism constitutive equation for cerebral arterial tissue, *International Journal of Solids and Structures* **46** 2920–2928 (2009).

[15] D. Li and A. M. Robertson, A structural multi-mechanism damage model for cerebral arterial tissue, *J. Biomech. Eng.* **131** 101–013 (2009).

[16] W. E. Stehbens, Histopathology of cerebral aneurysms. *Arch. Neurol.* **8**(3) 272–285 (1963).

[17] S. Scott, G. G. Ferguson, and M. Roach, Comparison of the elastic properties of human intracranial arteries and aneurysms. *J. Physiol. Pharmacol.* **50** 328–332 (1972).

[18] T. E. Carew, R. N. Vaishnav, and D. J. Patel, Compressibility of the arterial wall. *Circ. Res.* **23** 61–68 (1968).

[19] S. K. Kyriacou and J. D. Humphrey, Influence of size, shape and properties on the mechanics of axisymmetric saccular aneurysms. *J. Biomech.* **29**(8) 1015–1022 (1996).

[20] J. Bonet and R. D. Wood, Non-linear continuum mechanics for finite element analysis. *Cambridge University Press.* (1997).

[21] P. Neff and S. Hartman, Polyconvexity of generalized polynomial-type hyperelastic strain energy functions for near-incompressibility. *International Journal of Solids and Structures* **40** 2767–2791 (2003).

[22] G. A. Holzapfel and T. C. Gasser, A new constitutive framework for arterial wall mechanics and a comparative study of material models. *Journal of Elasticity* **61** 1–48 (2000).

[23] G. A. Holzapfel, Non-linear solid mechanics: A continuum approach for engineering. *Wiley, John & Sons, Incorporated* (2000).

[24] J. C. Simo, On a fully three-dimensional finite-strain viscoelastic damage model: formulation and computational aspects. *Computer Methods in Applied Mechanics and Engineering* **60**(2) 153–173 (1987).

[25] P. Le Tallec, Numerical methods for non-linear three-dimensional elasticity. In *Handbook of Numerical Analysis* **Vol. III** Elsevier Science (1994).

[26] R. W. Ogden, Non-linear elastic deformations, *Dover publications*, (1984).

[27] O. C. Zienkiewicz and R. C. Taylor, The finite element method, 4th Edition, *McGraw Hill*, **Vol. I** (1989), **Vol. II** (1991).

[28] M. de Luca, Mathematical and Numerical Models for cerebral aneurysm wall mechanics. *PhD Thesys, Politecnico di Milano* (2009).

[29] www.lifev.org.